

Long life of Gauss-Bonnet corrected black holes

R. A. Konoplya*

Department of Physics, Kyoto University, Kyoto 606-8501, Japan
&

*Theoretical Astrophysics, Eberhard-Karls University of Tübingen,
Tübingen 72076, Germany*

A. Zhidenko†

*Instituto de Física, Universidade de São Paulo,
C.P. 66318, 05315-970, São Paulo-SP, Brazil*

Dictated by the string theory and various higher dimensional scenarios, black holes in $D > 4$ -dimensional space-times must have higher curvature corrections. The first and dominant term is quadratic in curvature, and called the Gauss-Bonnet (GB) term. We shall show that although the Gauss-Bonnet correction changes black hole's geometry only softly, the emission of gravitons is suppressed by many orders even at quite small values of the GB coupling. The huge suppression of the graviton emission is due to the multiplication of the two effects: the quick cooling of the black hole when one turns on the GB coupling and the exponential decreasing of the grey-body factor of the tensor type of gravitons at small and moderate energies. At higher D the tensor gravitons emission is dominant, so that the overall lifetime of black holes with Gauss-Bonnet corrections is many orders larger than it was expected. This effect should be relevant for the future experiments in the Large Hadron Collider (LHC).

PACS numbers: 04.30.Nk, 04.50.+h

I. INTRODUCTION

During the past decade high energy physics got a great impact from theories implying existence of extra dimensions in the world. These are the string theory [1] and higher dimensional brane-world scenarios [2]. The low energy limit of the string theory can be described by the slope expansion in powers of the inverse string tension (or of the inverse square of the fundamental string scale ℓ_s^{-2}), what produces higher curvature corrections to the Einstein action. The quadratic term in curvature (given by the so-called Gauss-Bonnet invariant) is the leading correction that can affect the graviton excitation spectrum near the flat space.

The extra dimensional scenarios also suggest that the fundamental gravity scale M_* might be around the weak scale $\sim TeV$. Thus, at particle collisions with the cross-section $\sim \pi r_s^2$, where r_s is the Schwarzschild radius, and energies larger than M_* , the production of mini-black holes should start. These black holes are intrinsically higher dimensional and usually modeled by the Tangherlini metric, which is the solution of the D-dimensional Einstein equations. However, in order to have a mathematically non-contradictory gravity in higher dimensions, one has to take account of higher curvature corrections of the same form as those appearing in the slope expansion of the string theory. The spherically symmetric solution describing neutral static black holes in the D-

dimensional Einstein gravity with the GB corrections was obtained in [3]. This solution contains small corrections to the D-dimensional Schwarzschild-Tangherlini geometry and consequently properties of such Gauss-Bonnet corrected black holes were expected to differ only slightly from the Schwarzschild's ones. This happens, for instance, for the spectrum of proper oscillations of these black holes [4].

Unlike astrophysical black holes, whose Hawking evaporation is negligibly small, mini-black holes are intensively evaporating what leads to the very short lifetime of these black holes, once they are created. The latter is due to strong production of various particles from the vacuum around a black hole and emission of them through the mechanism of Hawking radiation [5]. At large number of space-time dimensions D , the specific “tensorial” type of gravitons (respectively the $D - 2$ rotation group) dominates in the emission process [13]. Up to now, an impressively extensive literature is devoted to the calculations of Hawking evaporation of the Schwarzschild-Tangherlini and Myers-Perry black holes [6–10], while evaporation of their higher curvature corrected generalizations was touched only in a couple of works [11, 12]. In particular, T. Rizzo estimated the energy-emission rate for the higher curvature corrected black holes, assuming that the grey body factor equals unity [11]. This was expected to give the correct answer about the order of the intensity of the Hawking emission. Though, as we shall show in this paper, the contribution due to the grey-body factors can also considerably change the results. In [12], the scattering of Standard Model particles around Gauss-Bonnet black holes was considered, though the calculations were terminated at the grey-body

*Electronic address: konoplya_roma@yahoo.com

†Electronic address: zhidenko@fma.if.usp.br

factors and the numbers of particles per frequency. Thus, none of the above works calculated the energy-emission rate for Gauss-Bonnet black holes, what is necessary for the estimation of the total emission of energy and thus of the black hole lifetime. Here we shall fill this gap and calculate of the energy-emission rates for fields of various spin, including gravitons, and thus shall estimate lifetime of Gauss-Bonnet black holes.

In this work, we shall show that due to a number of reasons, the emission of tensor type of gravitons is greatly (in fact exponentially) suppressed when one turns on the GB coupling α' . Thus, even at small values of the GB coupling constant α' *the graviton emission is suppressed by many orders*. This means that small GB corrections lead to much longer life of higher dimensional black holes, than it was expected [13–15]. At the first sight this enormous suppression would not seem trustable: why slight corrections of geometry produce very strong effect on evaporation process? The reasons for this are “multiplication” of the two factors. First, the black hole get much colder when one turns on the GB coupling and the

emission rate is quadratic in temperature. Second, the emission is proportional to the grey-body factor which is exponentially suppressed for tensorial gravitons. This explanation certainly did not make us trust the result immediately. Therefore we reproduced our accurate numerical calculations by the semi-analytical WKB estimations.

The paper is organized as follows: Sec II briefly discuss the deduction of wave equations for perturbations of fields of various spin. Sec III is devoted to numerical calculation of the coefficients of transmission, while Sec. IIIB gives WKB values of the coefficients. In Sec. IV the obtained scattering data is used for the calculations of the energy-emission rates. Using the WKB arguments Sec. V explains why the found enormous suppression of Hawking evaporation occurs. In Sec. VI we estimate the lifetime of Gauss-Bonnet corrected black holes and outline the future perspective of this direction.

We shall consider the canonical ensemble, which leads to the same results as the microcanonical one if the black hole mass M is at least a few times larger than M_* [11].

II. THE WAVE LIKE EQUATIONS

A. Gravitational perturbations

The Einstein-Gauss-Bonnet action is

$$I = \frac{1}{16\pi G_D} \int d^D x \sqrt{-g} R + \alpha' \int d^D x \sqrt{-g} (R_{abcd} R^{abcd} - 4R_{cd} R^{cd} + R^2), \quad (1)$$

where α' is the coupling constant; $\alpha' = 1/2\pi\ell_s^2$. The metric has the form,

$$ds^2 = f(r)dt^2 - \frac{dr^2}{f(r)} - r^2 d\Omega_{D-2}^2, \quad (2)$$

$$f(r) = 1 + \frac{r^2(1-q(r))}{\alpha(D-3)(D-4)}, \quad q(r) = \sqrt{1 + \frac{4\alpha(D-3)(D-4)\mu}{(D-2)r^{D-1}}} \quad (3)$$

where $d\Omega_{D-2}^2$ is the line element of a unit $(D-2)$ -sphere and $\alpha = 16\pi G_D \alpha'$. As we mentioned earlier, we shall measure all quantities in terms of the black hole horizon radius, which we shall denote as r_0 , so that the black hole mass can be written as

$$\mu = \frac{(D-2)r_0^{D-3}}{4} \left(2 + \frac{\alpha(D-3)(D-4)}{r_0^2} \right). \quad (4)$$

The linearized perturbations of (2) can be written in the general form as

$$g_{ab} \rightarrow g_{ab} + \delta g_{ab} = g_{ab} + h_{ab}. \quad (5)$$

Indices of h_{ab} are raised using the background metric, therefore

$$\delta g^{ab} = -h^{ab}.$$

The first order variation of the Riemann tensors is:

$$\delta R_{ab}{}^{cd} = \frac{1}{2} \left\{ R_{ab}{}^{df} h_f{}^c - R_{ab}{}^{cf} h_f{}^d + \left(\nabla_b \nabla^c h_a{}^d - \nabla_a \nabla^c h_b{}^d \right) + \left(\nabla_a \nabla^d h_b{}^c - \nabla_b \nabla^d h_a{}^c \right) \right\}. \quad (6)$$

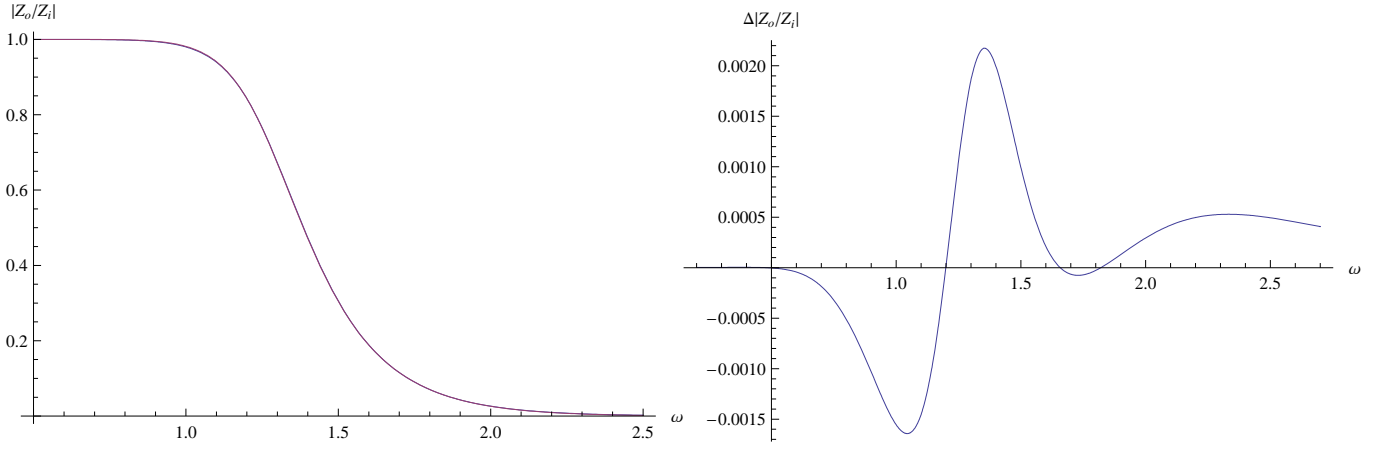


FIG. 1: Square root of the reflection coefficient $|Z_o/Z_i|$ for $D = 6$, $\alpha = 2$, $l = 2$ tensor-type gravitational perturbations. On the left figure we show the coefficient calculated by fitting the numerically solved equation (blue) and using the 6-th order WKB formula (red). On the right figure we plot the difference between the coefficients calculated using these two methods.

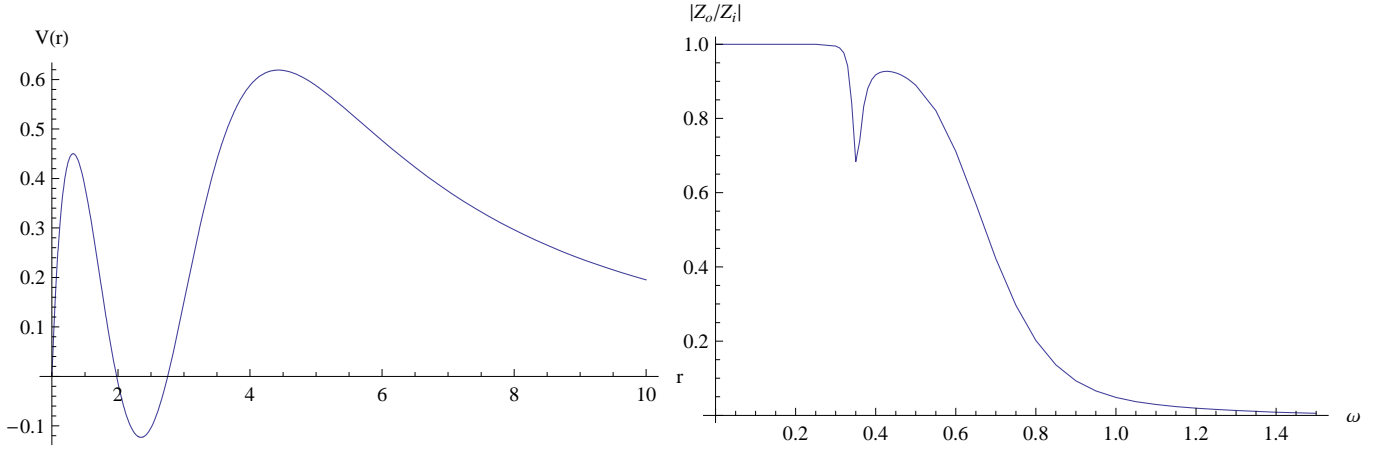


FIG. 2: The effective potential $V(r)$ (left figure) and the square root of the reflection coefficient $|Z_o/Z_i|$ for $D = 6$, $\alpha = 2$, $l = 2$ scalar-type gravitational perturbations.

Using the symmetry of the background metric, one can decompose the perturbation equations into scalars, vectors and tensors according to rotation group on the $(D - 2)$ -sphere [20]. Then, the separation of angular variables is possible for this case [20].

After separation of the angular variables and implying stationarity, $\Psi(t, r) = e^{-i\omega t}\Phi(r)$, the dynamics of the gravitational perturbations can be reduced to the wave-like equations [20],

$$\left(\frac{d^2}{dr_\star^2} + \omega^2 - V_i(r) \right) \Phi_i(r) = 0, \quad dr_\star = \frac{dr}{f(r)}, \quad (7)$$

with the effective potentials which have very cumbersome form. After some algebra, we managed to simplify the potentials obtained by Dotti and collaborators in [20] for the tensor, vector and scalar types of the gravitational perturbation respectively:

$$V_T(r) = f(r) \frac{\lambda}{r^2} \left(3 - \frac{B(r)}{A(r)} \right) + \frac{1}{\sqrt{r^{D-2} A(r) q(r)}} \frac{d^2}{dr_*^2} \sqrt{r^{D-2} A(r) q(r)}, \quad (8)$$

$$V_V(r) = f(r) \frac{(D-2)c}{r^2} A(r) + \sqrt{r^{D-2} A(r) q(r)} \frac{d^2}{dr_*^2} \frac{1}{\sqrt{r^{D-2} A(r) q(r)}}, \quad (9)$$

$$V_S(r) = \frac{f(r) U(r)}{64r^2 (D-3)^2 A(r)^2 q(r)^8 (4cq(r) + (D-1)R(q(r)^2 - 1))^2}. \quad (10)$$

Here we used the following dimensionless quantities

$$\begin{aligned} A(r) &= \frac{1}{q(r)^2} \left(\frac{1}{2} + \frac{1}{D-3} \right) + \left(\frac{1}{2} - \frac{1}{D-3} \right), \\ B(r) &= A(r)^2 \left(1 + \frac{1}{D-4} \right) + \left(1 - \frac{1}{D-4} \right), \\ R &= \frac{r^2}{\alpha(D-3)(D-4)}, \end{aligned}$$

$$\begin{aligned} U(r) &= 5(D-1)^6 R^2 (1+R) - 3(D-1)^5 R ((D-1)R^2 + 24c(1+R))q(r) + \\ &+ 2(D-1)^4 (24c(D-1)R^2 + 168c^2(1+R) - (D-1)R^2(-3+5R+7D(1+R)))q(r)^2 + \\ &+ 2(D-1)^4 R(-184c^2 + (D-1)(13+D)R^2 + c(-84+44R+84D(1+R)))q(r)^3 + \\ &+ (D-1)^3 (384c^3 - 48c(2+D(3D-5))R^2 + 192c^2(-11+D+(-15+D)R) + \\ &+ (D-1)R^2(-3(7+55R) + D(26+106R+7D(1+R))))q(r)^4 + \\ &+ (D-1)^3 R(-64c^2(D-38) + (D-1)(71+D(7D-90))R^2 + \\ &+ 16c(303+255R+13D^2(1+R) - 2D(73+81R)))q(r)^5 + \\ &+ 4(D-1)^2 (96c^3(-7+D) - 8c(D-1)(145-74D+6D^2)R^2 - \\ &- 8c^2(9-175R+D(-58-34R+11D(1+R))) + (D-1)R^2(-5(79+23R) + \\ &+ D(5(57+41R) + D(-81-89R+7D(1+R))))q(r)^6 - \\ &- 4(D-1)^2 R(8c^2(43+(72-13D)D) + (D-1)(-63+D(99+D(-49+5D))))R^2 + \\ &+ 4c(321+465R+D(121-39R+D(-123-107R+17D(1+R))))q(r)^7 + \\ &+ (D-1)(128c^3(-9+D)(D-5) + 32c(D-1)(246+D(9+D(-55+8D))))R^2 + \\ &+ 64c^2(D-5)(D^2-3+(49+(D-4)D)R) - (D-1)R^2(1173+565R+ \\ &+ D(-4(997+349R) + D(6(393+217R) + D(-548-452R+45D(1+R))))q(r)^8 + \\ &+ (D-1)R(-64c^2(D-5)(36+D(-13+3D)) + \\ &+ (D-1)(635+D(-1204+3D(294+D(-92+9D))))R^2 - \\ &- 8c(D-5)(63+31R+D(127+191R+D(-47+D+(-79+D)R)))q(r)^9 + \\ &+ 2(D-5)(64c^3(D-5)(D-3) + 8c(D-1)(-27+D(141+(-43+D)D)))R^2 + \\ &+ 8c^2(D-5)(-3+77R+D(D-2+(D-18)R)) + (D-1)^2 R^2(-33(R-7) + \\ &+ D(59+43R+D(-59-35R+9D(1+R))))q(r)^{10} - \\ &- 2(D-5)R(24c^2(-11+D)(D-5)(D-3) + (D-1)^2(-65+D(81+D(7D-39))))R^2 + \\ &+ 12c(-7+D)(D-5)(D-3)(D-1)(1+R))q(r)^{11} + \\ &+ (D-5)^2(-1+D)R^2(16c(26+(D-9)D) + \\ &+ (D-1)(77-3R+D(-18+D+(D-2)R)))q(r)^{12} + \\ &+ (D-5)^2(D-3)^2(D-1)^2 R^3 q(r)^{13}, \end{aligned}$$

$\lambda = (D-2)(c+1) = \ell(\ell+D-3)$ is the eigenvalue of the angular part of the Laplacian, $\ell = 2, 3, 4, \dots$

A wide class of static black holes in the Einstein gravity is known to be stable against gravitational perturbations for any number of space-time dimensions [19]. This is not true for black holes in the Einstein-Gauss-Bonnet theory which suffer from instability for sufficiently large (in units of the radius of the event horizon) values of the GB coupling

α [20, 21]. We shall consider here only small enough values of the GB coupling α which are below the threshold of the gravitational instability [20, 22]. In other words, we shall be limited by not very small masses of black holes M , which usually are at least one order larger than M_* .

B. Test scalar field

We shall also consider the test scalar field in the background (2) which satisfies the Klein-Gordon equation

$$\nabla^a \nabla_a \Phi = 0. \quad (11)$$

After separation of the angular variables the equation (11) can be reduced to the wave-like form (7) with the following effective potential

$$V_{SB}(r) = f(r) \left(\frac{\lambda}{r^2} + \frac{(D-2)(D-4)}{4r^2} f(r) + \frac{(D-2)}{2r} f'(r) \right), \quad (12)$$

where $\lambda = \ell(\ell + D - 3)$, $\ell = 0, 1, 2, 3, \dots$

Let us note, that unlike the Schwarzschild black hole, the Gauss-Bonnet black hole has the effective potential for the scalar field (12) which differs from the effective potentials for the tensor-type gravitational perturbations (8). In the limit $\alpha \rightarrow 0$ (12) coincides with (8).

C. Brane-localized fields

In addition, we shall consider the Standard Model fields (scalars, fermions and gauge bosons) living on a 4-dimensional brane, which is embedded in the background of the Gauss-Bonnet black hole. The induced metric on the brane is given by a projection of the metric (2) onto the 4-brane [23]

$$ds^2 = f(r)dt^2 - \frac{dr^2}{f(r)} - r^2 d\Omega_2^2, \quad (13)$$

where $d\Omega_2^2$ is the line element of a unit sphere.

The effective potential for the scalar field (11) in the metric (13) is

$$V_{SP}(r) = f(r) \left(\frac{\ell(\ell + 1)}{r^2} + \frac{f'(r)}{r} \right). \quad (14)$$

The massless gauge field satisfies the equation

$$\nabla^a (\nabla_a A_b - \nabla_b A_a) = 0. \quad (15)$$

After the separation of the angular variables, one can find the effective potential for the two types of the polarizations

$$V_{GP}(r) = f(r) \frac{\ell(\ell + 1)}{r^2}, \quad (16)$$

where $\ell = 1, 2, 3, \dots$

For the fermions we do not consider the equation in the standard Schrodinger wave-like form because of the boundary conditions: we will calculate the grey-body factors for neutrinos and anti-neutrinos using the approach of [24]. That is why we use here the equation for the radial part in the following form

$$\Delta(r)\Psi''(r) + \frac{\Delta'(r)}{2}\Psi'(r) + \left(\frac{2\omega^2 r^4 - i\omega r^2 \Delta'(r)}{2\Delta(r)} + 2i\omega r - \kappa^2 \right) \Psi(r) = 0, \quad (17)$$

where $\Delta(r) = r^2 f(r)$ and $\kappa = 1, 2, 3, \dots$

III. CALCULATIONS OF THE ENERGY-EMISSION RATE

In order to calculate the intensity of the Hawking radiation, one should first calculate the gray-body factors,

that is, to solve the problem of classical scattering around

black holes with pure in-going boundary conditions at the event horizon. The latter is reduced to the finding of the S-matrix, or, simply, of the reflection or the transmission coefficients.

A. Reflection coefficients

At the event horizon we impose the boundary condition which correspond to the purely ingoing wave

$$\Phi(r) \propto e^{-i\omega r_*} \propto (r - r_0)^{-i\omega/f'(r_0)}. \quad (18)$$

At the spatial infinity ($r \rightarrow \infty$) the two linearly independent solutions of the wave-like equation (7) are

$$\Phi(r) \simeq Z_i \exp(-i\omega r_*) + Z_o \exp(i\omega r_*),$$

where Z_i and Z_o are integration constants which correspond to the ingoing and outgoing waves respectively. Introducing the new function

$$P(r) = (1 - (r_0/r))^{i\omega/f'(r_0)} \Phi(r),$$

and choosing the integration constant as $P(r_0) = 1$, we expand the equation (7) near the event horizon and find $P'(r_0)$, which completely determines initial conditions for the numerical integration. Then, we integrate numerically the equation (7) from the event horizon r_0 until some distant point $R \gg r_0$ and find a fit for the numerical solution far from the black hole in the form

$$P(r) = Z_i P_i(r) + Z_o P_o(r), \quad (19)$$

where the asymptotical expansions for the corresponding functions are found by expanding (7) for large r as

$$\begin{aligned} P_i(r) &= e^{-i\omega r} \left(1 + P_i^{(1)} r^{-1} + P_i^{(2)} r^{-2} + \dots \right), \\ P_o(r) &= e^{i\omega r} \left(1 + P_o^{(1)} r^{-1} + P_o^{(2)} r^{-2} + \dots \right). \end{aligned}$$

The fitting procedure allows us to find the coefficients Z_i and Z_o . In order to check the accuracy of the calculated coefficients one should increase the internal precision of the numerical integration procedure, the value of R and the number of terms in the series expansion for $P_i(r)$ and $P_o(r)$, making sure that the values of Z_i and Z_o do not change within the desired precision.

B. WKB approach

Another way to check our numerical calculations is to compare the fraction Z_o/Z_i with the result provided by the 6-th order WKB method, which gives quite an accurate answer for large and moderate values of ℓ [16]. The WKB approach was initially used for finding quasinormal modes for which it usually provides quite a good accuracy at the 6th order [18]

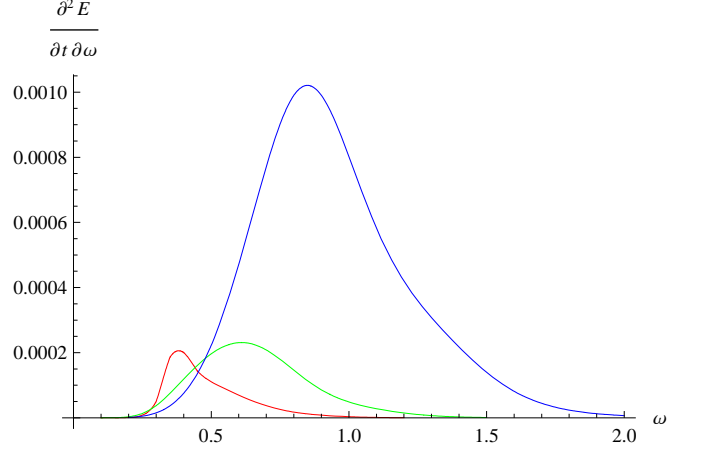


FIG. 3: The energy-emission rates for the Gauss-Bonnet black holes $D = 6$, $\alpha = 1/5$ (blue, top line), $\alpha = 1/2$ (green line), $\alpha = 1$ (red, bottom line).

The reflection coefficient, given by the WKB formula, is

$$|Z_o/Z_i|^2 = (1 + e^{-2i\pi K})^{-1}, \quad (20)$$

where

$$K = i \frac{(\omega^2 - V_0)}{\sqrt{-2V_0''}} + \sum_{i=2}^{i=6} \Lambda_i. \quad (21)$$

Here V_0 is the maximum of the effective potential, V_0'' is the second derivative of the effective potential in its maximum with respect to the tortoise coordinate, and Λ_i are higher order WKB corrections which depend on up to $2i$ -th order derivatives of the effective potential at its maximum.

From the Fig. 1 we see that the difference between the results, found by these two methods is a fraction of a percent. Unfortunately, for some values of the parameters the effective potential does not have a form of a peak (see Fig. 2). In these cases the WKB formula cannot be used in the present form. That is why, despite in most cases the WKB formula provides a good approximation, we use numerical integration procedure which works for any form of the effective potential.

C. Graviton emission

When the coefficients Z_i and Z_o are obtained, one can find the absorption probability

$$|\mathcal{A}_\ell|^2 = 1 - |Z_o/Z_i|^2 \quad (22)$$

and, then, the energy-emission rate

$$\frac{dE}{dt} = \sum_{\ell} N_{\ell} |\mathcal{A}_{\ell}|^2 \frac{\omega}{\exp(\omega/T_H) - 1} \frac{d\omega}{2\pi}, \quad (23)$$

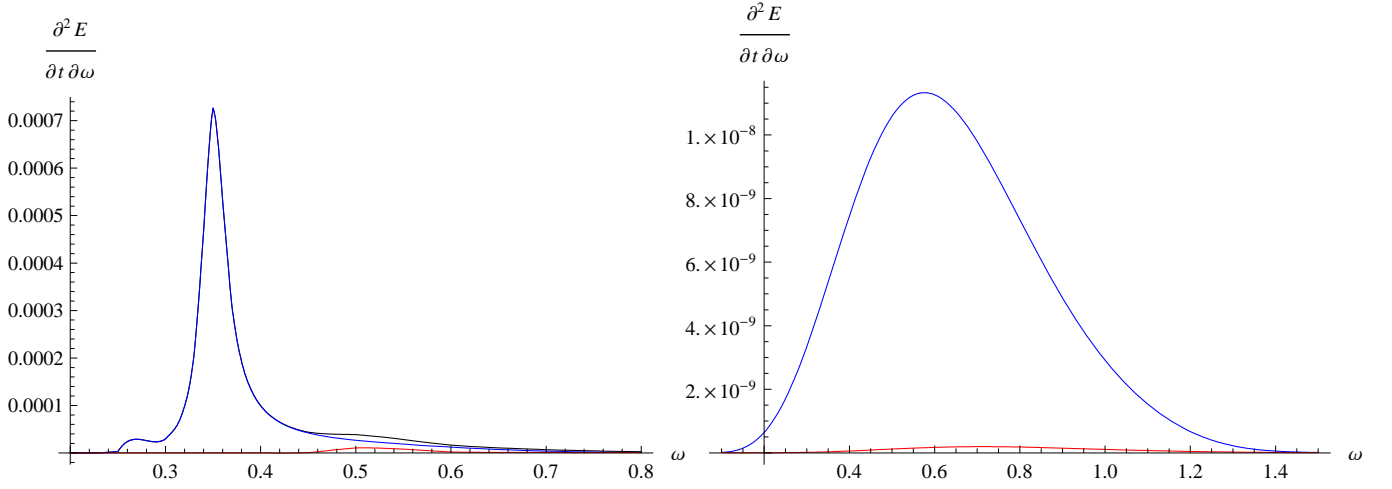


FIG. 4: The energy-emission rate (left figure) and the contribution of the graviton emission of tensor type (right figure) for the Gauss-Bonnet black hole $D = 6$, $\alpha = 2$. Blue (top) and red (bottom) lines correspond respectively to the contribution of $l = 2$ and $l = 3$ multipoles of scalar type (left figure) and of tensor type (right figure).

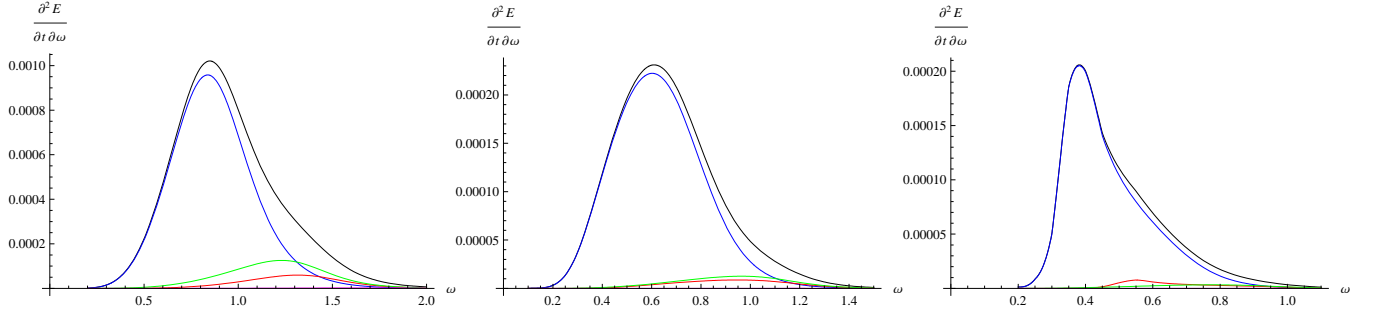


FIG. 5: The energy-emission rates (black line) for the Gauss-Bonnet black holes $D = 6$, $\alpha = 1/5, 1/2, 1$ (from left to right) together with contributions of different type of gravitons (color lines): $l = 2$ scalar type (blue, top), $l = 2$ vector type (green), $l = 3$ scalar type (red), $l = 2$ tensor type (magenta, bottom).

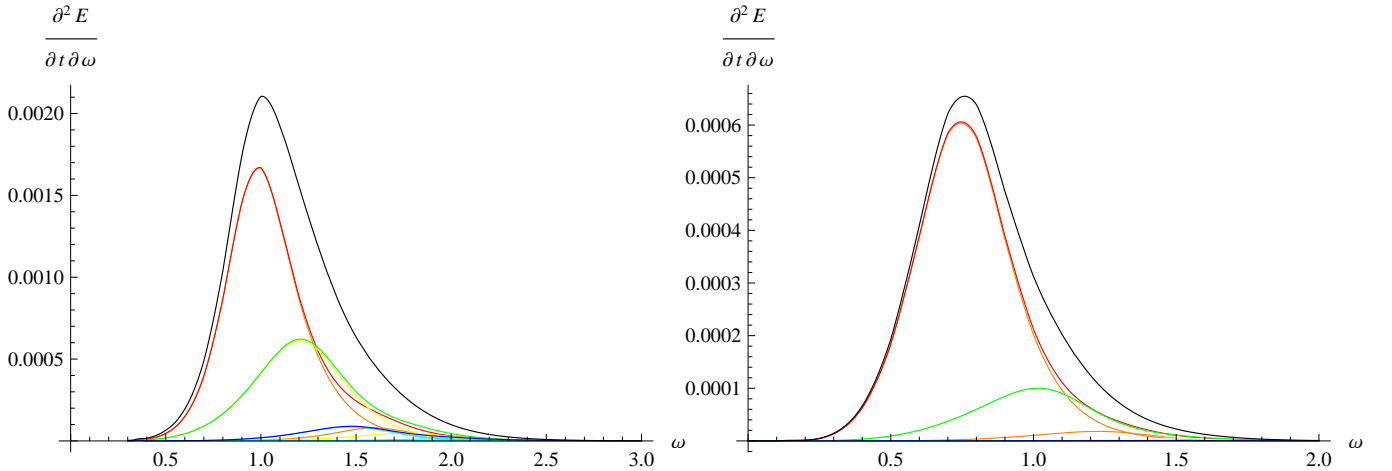


FIG. 6: The energy-emission rates for $D = 5$ Schwarzschild (left figure) and Gauss-Bonnet black holes ($\alpha = 1/5$, right figure). The black line is the total energy-emission rate. Scalar-type, vector-type and tensor-type gravitons' contributions are red, green and blue. The contributions of the corresponding multipole numbers are orange, yellow and cyan. The largest gravitons' contribution is of scalar-type, the smallest is of tensor-type.

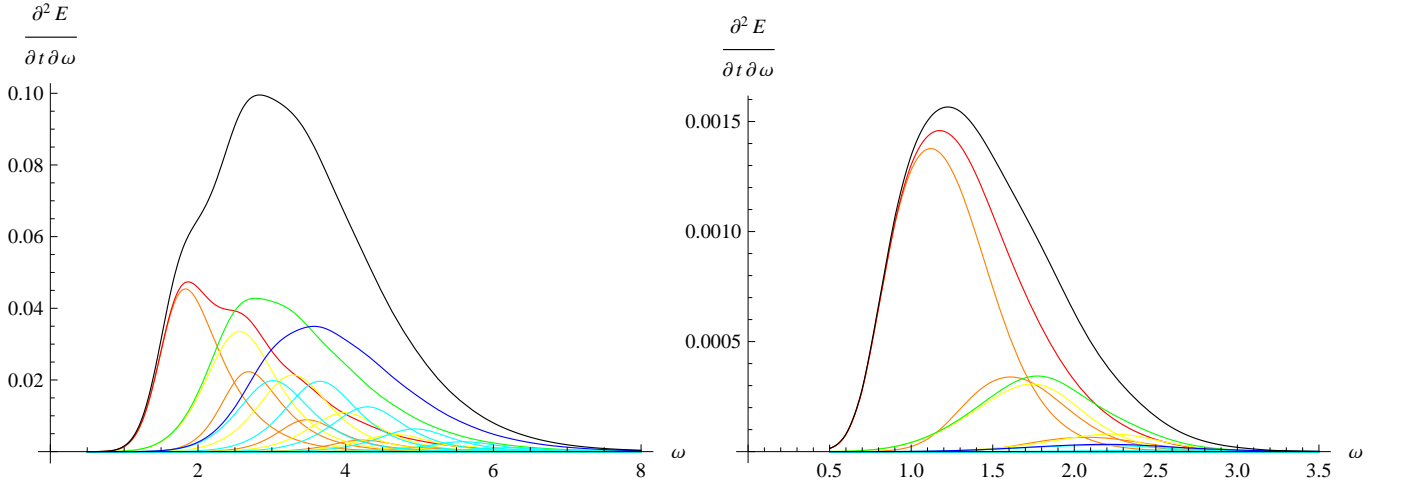


FIG. 7: The energy-emission rates for $D = 8$ Schwarzschild (left figure) and Gauss-Bonnet black holes ($\alpha = 1/5$, right figure). The black line is the total energy-emission rate. Scalar-type, vector-type and tensor-type gravitons' contributions are red, green and blue. The contributions of the corresponding multipole numbers are orange, yellow and cyan. The largest gravitons' contribution is of scalar-type, the smallest is of tensor-type.

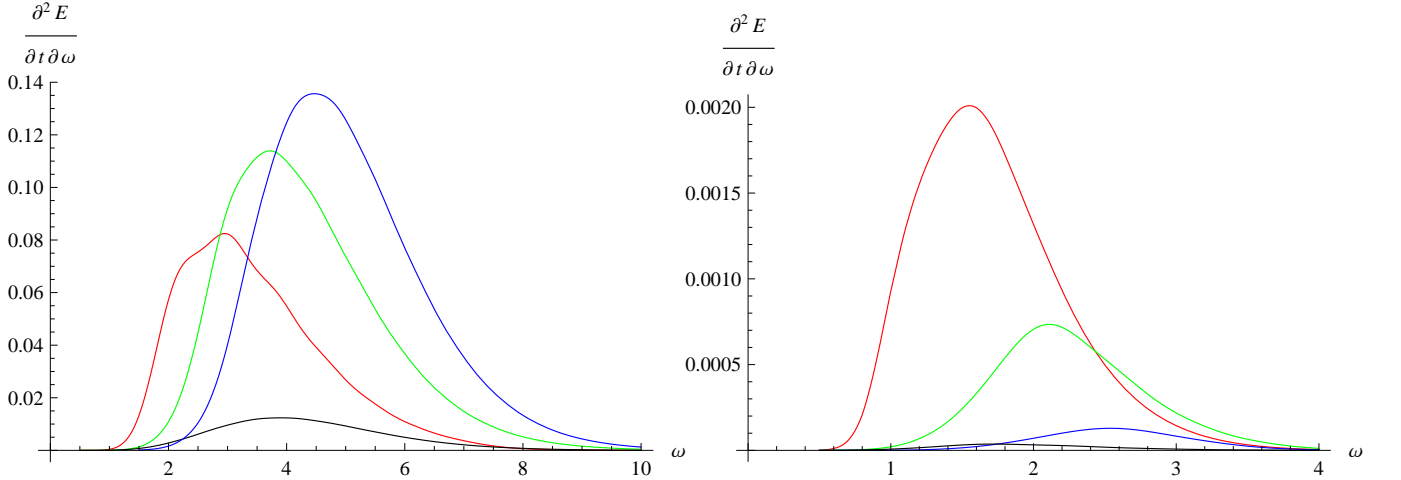


FIG. 8: The energy-emission rates for $D = 9$ Schwarzschild (left figure) and Gauss-Bonnet black holes ($\alpha = 1/5$, right figure). Scalar-type, vector-type and tensor-type gravitons' emission rates are red, green and blue. For the Schwarzschild black hole the largest gravitons' contribution is of tensor-type and the smallest is of scalar-type, while for $\alpha = 1/5$ Gauss-Bonnet black hole the largest gravitons' contribution is of scalar-type and the smallest is of tensor-type. The black (bottom) line is the energy-emission rate due to the scalar field.

where the multiplicity factors N_ℓ are [15]

$$N_\ell^{(T)} = \frac{(D-1)(\ell+D-2)(\ell-1)(2\ell+D-3)(\ell+D-5)!}{2(\ell+1)!(D-3)(D-5)!},$$

$$N_\ell^{(V)} = \frac{(\ell+D-3)\ell(2\ell+D-3)(\ell+D-5)!}{(\ell+1)!(D-4)!},$$

$$N_\ell^{(S)} = \frac{(2\ell+D-3)(\ell+D-4)!}{\ell!(D-3)!},$$

for the gravitational perturbations of tensor, vector and scalar types. The Hawking temperature is

$$T_H = \frac{f'(r_0)}{4\pi} = \frac{(D-3)(2r_0^2 + \alpha(D-4)(D-5))}{8\pi r_0(r_0^2 + \alpha(D-3)(D-4))}.$$

D. Emission of the scalar field and the Standard Model fields

The scalar field living in the bulk has the same number of the degrees of freedom as the gravitational perturbations of scalar type

$$N_\ell^{(SB)} = \frac{(2\ell+D-3)(\ell+D-4)!}{\ell!(D-3)!}.$$

For the scalar field localized on the brane the multiplicity factor is given

$$N_\ell^{(SP)} = \frac{(2\ell+1)\ell!}{\ell!1!} = 2\ell+1.$$

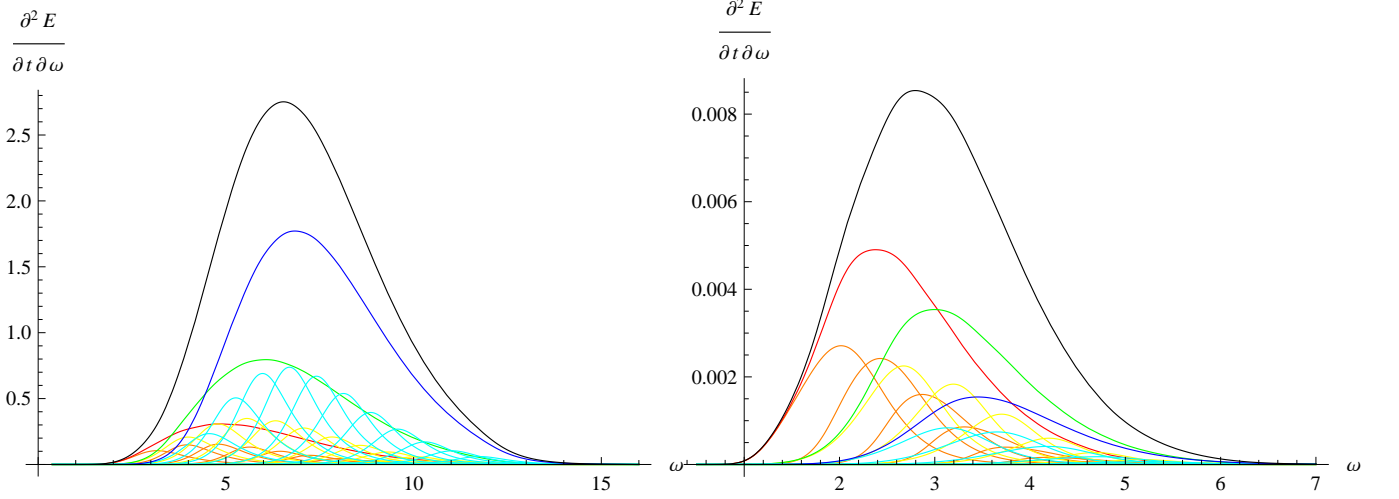


FIG. 9: The energy-emission rates for $D = 11$ Schwarzschild (left figure) and Gauss-Bonnet black holes ($\alpha = 1/5$, right figure). The black line is the total energy-emission rate. Scalar-type, vector-type and tensor-type gravitons' contributions are red, green and blue. The contributions of the corresponding multipole numbers are orange, yellow and cyan. For the Schwarzschild black hole the largest gravitons' contribution is of tensor-type and the smallest is of scalar-type, while for $\alpha = 1/5$ Gauss-Bonnet black hole the largest gravitons' contribution is of scalar-type and the smallest is of tensor-type.

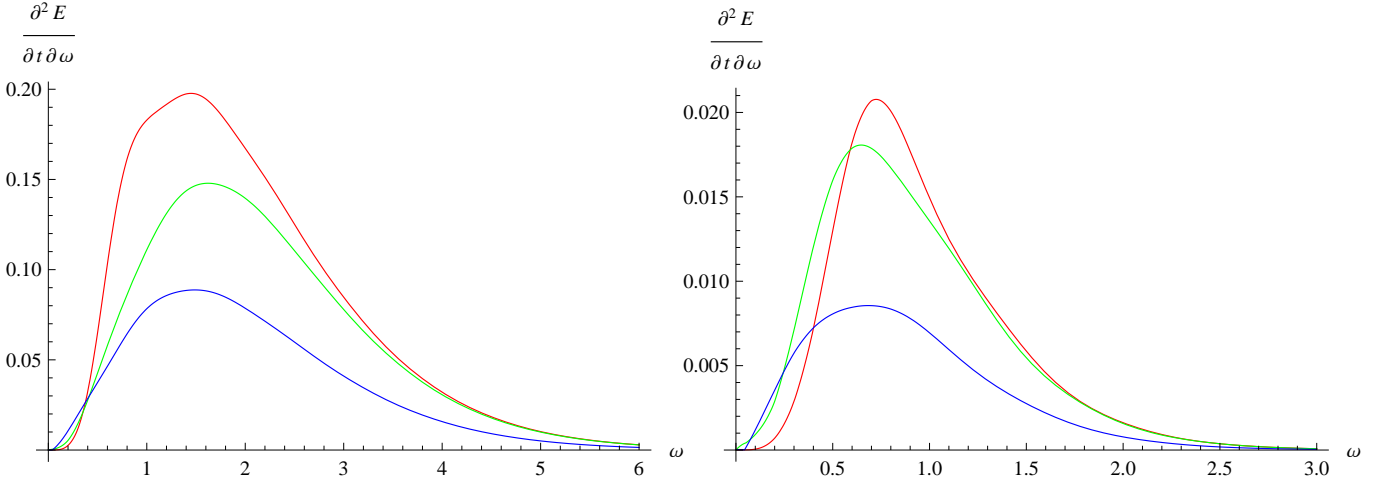


FIG. 10: The energy-emission rates for $D = 10$ Schwarzschild (left figure) and Gauss-Bonnet black holes ($\alpha = 1/5$, right figure) due to brane-localized fields: gauge (red, top), Dirac (green) and scalar (blue, bottom).

For the gauge field the multiplicity factor is the same for each polarization

$$N_{\ell}^{(GP)} = 2\ell + 1.$$

For the neutrinos and antineutrinos the multiplicity factor is

$$N_{\kappa}^{(FP)} = 2\kappa$$

In order to calculate the absorption probability for the fermions we use the approach of [24]

$$|\mathcal{A}_{\kappa}|^2 = 1 - \frac{4\omega^2}{\kappa^2} \left| \frac{Z_o}{Z_i} \right|^2.$$

The energy-emission rate for the neutrinos and antineutrinos is the same and given by

$$\frac{dE}{dt} = \sum_{\kappa=1}^{\infty} N_{\kappa}^{(FP)} |\mathcal{A}_{\kappa}|^2 \frac{\omega}{\exp(\omega/T_H) + 1} \frac{d\omega}{2\pi}.$$

Note that we take into account contributions of neutrinos and antineutrinos and both polarizations of the gauge bosons. That is why our result is two times larger than in [13].

TABLE I: Energy-emission rate for Schwarzschild (first line) and Schwarzschild-Gauss-Bonnet ($\alpha/r_0^2 = 1/5$) (second line) black holes.

D	gravitational				scalar field		projected SM fields	
	total	scalar	vector	tensor	bulk	projected	$s = 1/2$	$s = 1$
5	0.00133	0.00085	0.00041	0.00006	0.00105	0.00266	0.00464	0.00365
	0.000322	0.000267	0.000055	0.000001	0.000230	0.000772	0.001259	0.000733
6	0.01380	0.00796	0.00437	0.00147	0.00267	0.01073	0.01955	0.01944
	0.000618	0.000535	0.000082	0.000002	0.000100	0.001141	0.002051	0.001340
7	0.06942	0.03229	0.02366	0.01347	0.00648	0.02972	0.05310	0.05935
	0.000994	0.000833	0.000152	0.000008	0.000057	0.001832	0.003440	0.002528
8	0.27143	0.09152	0.09648	0.08343	0.01614	0.06613	0.11527	0.13742
	0.001737	0.001366	0.000332	0.000038	0.000047	0.003197	0.006157	0.005043
9	0.9975	0.2294	0.3440	0.4241	0.04216	0.12769	0.21768	0.26977
	0.003490	0.002430	0.000897	0.000162	0.000050	0.005631	0.010781	0.009809
10	3.6665	0.5592	1.1639	1.9434	0.11595	0.22321	0.37362	0.47460
	0.007727	0.004550	0.002425	0.000752	0.000064	0.009633	0.018190	0.017976
11	13.7745	1.4696	3.8936	8.4113	0.34326	0.36257	0.59793	0.77210
	0.018552	0.008939	0.006678	0.002935	0.000094	0.015795	0.029331	0.030885

IV. RESULTS

On Fig. 3 one can see that the energy emission rate per unit frequency ω for gravitons strongly decreases as α/r_0^2 increases, leading to suppression of about five times for $\alpha/r_0^2 = 1$. Examples of contributions of various multipoles and of various types of gravitons (scalar, vector and tensor) are given on Figs. 4, 5, 6, 7, 8, 9. These are given for $D = 6$ as an example, while from the table I, we can see the relative contributions for all types of particles for various number of space-time dimensions. On Fig. 10 one can see contributions of brane-localized Standard model fields into the energy emission rate: for $D \geq 6$ the larger spin of a field, the larger is the corresponding energy emission rate per unit frequency around its maximum.

An important for our future discussion observation is about the role of the tensor type of gravitons in the evaporation process. For vanishing GB coupling the tensor type of gravitons corresponds to the highest energy emission rate, which leads to the dominance of tensorial gravitons among all particles in the Hawking radiation at large D (see Figs. 8, 9). For non zero α this is not true anymore: the energy emission rates of tensorial gravitons becomes strongly suppressed and the Standard Model particles dominate in the evaporation at high D .

Finally, let us justify here in more detail why we chose the units of the fixed event horizon and not the units of the fixed black hole mass.

First, we would like to mention that from the values in units of the black hole radius, using a simple formula which we shall show in the next section, we are always able to recalculate values of the energy-emission rate in units of the black hole mass or Planck mass. The inverse formula is not so simple because the mass appears in the left-hand side as well. Second, in order to calculate the energy-emission rate in units of the mass, we must fix in some way the real Planck mass, which we have not

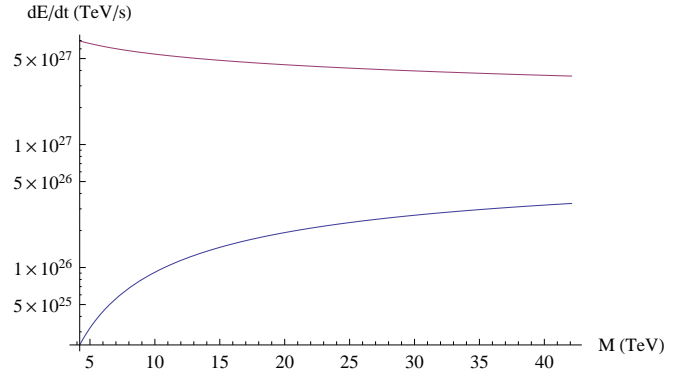


FIG. 11: The energy-emission rate as a function of mass M for $D = 10$ Schwarzschild (top) and $\alpha = 0.1 \text{TeV}^{-2}$ GB (bottom) black holes, $M_* = 1 \text{TeV}$. According to the recent experiments $M_* \geq 0.6 \text{TeV}$ (for $D = 10$) [14]. For larger M_* the plots are qualitatively the same.

known yet. Third, the purpose of the table I is to show that, independently on the new Planck mass, the energy-emission rate decreases some orders. This is a general result, which we would loose if we fix the Planck mass in some way. In order to show this effect we present a figure in the units of TeVs to illustrate how the emission rate depends on the back hole mass (Fig. 11).

V. DISCUSSIONS

From the Fig. 12 and Table I one can see that the energy-emission rate decreases quickly (in fact, almost exponentially) with α . In order to understand why this happens for relatively small corrections to the black hole geometry let us use the WKB approach and consider the cases of small and large ω of separately.

The numerical data, which we obtained here (table I), does not use the small ω expansion of [13] and is, thereby,

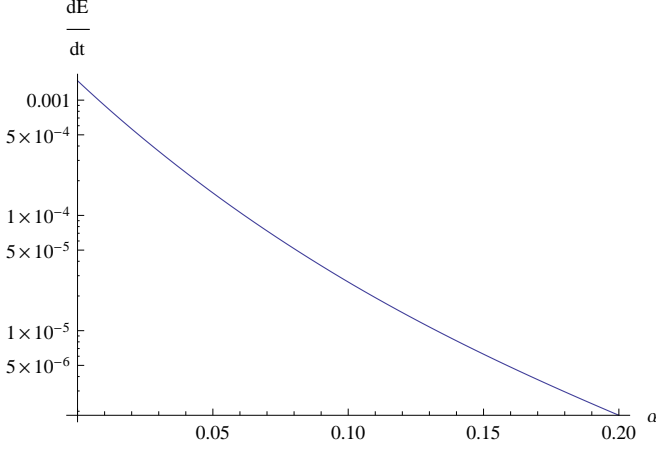


FIG. 12: Energy-emission rate of the tensor-type gravitons as a function of α for $D = 6$.

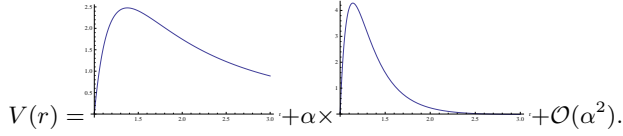


FIG. 13: Expansion of the tensor-type perturbation potential $D = 5$, $\ell = 2$.

more accurate.

When $\omega^2 < V_{max}$, the energy-emission rate decreases due to the suppression of the grey-body factor for tensor gravitons. In order to show this we use the WKB approximation. For $\omega^2 \ll V_{max}$ the WKB formula reads

$$|\mathcal{A}|^2 \approx \exp\left(-2 \int dr_* \sqrt{V(r_*) - \omega^2}\right), \quad (24)$$

where integration is performed between the two turning points $V(r_*) = \omega^2$. On the Fig. 13 we see that the leading order of α increases the height of the potential barrier, as well as the distance between the turning points. Then,

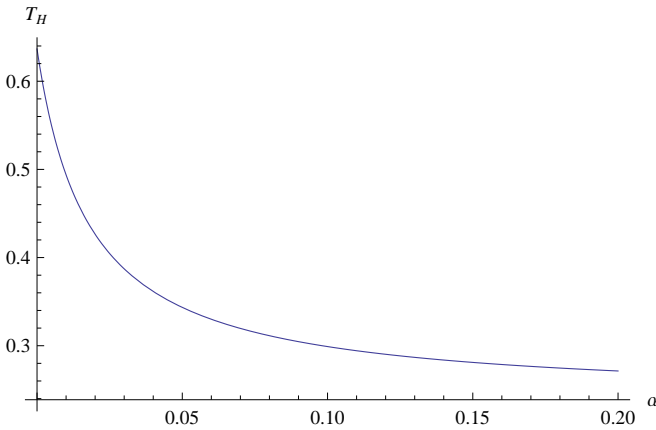


FIG. 14: Black hole temperature as a function of α for $D = 11$.

from (24) it is clear that the grey-body factor decreases exponentially as the effective potential for tensor gravitons grows.

In the eikonal approximation for $\omega^2 \lesssim V_{max}$ one has

$$|\mathcal{A}|^2 \approx \frac{e^{-2\pi(V_{max}-\omega^2)/\sqrt{-2V_{max}''}}}{1 + e^{-2\pi(V_{max}-\omega^2)/\sqrt{-2V_{max}''}}}.$$

As the height of the potential increases with growing of α , the dominant contribution comes from the numerator and the grey-body factor for tensor gravitons is

$$|\mathcal{A}|^2 \propto e^{-C(\omega)\alpha}, \quad C(\omega) > 0.$$

For large values of ω it is evident that $|\mathcal{A}|^2 \approx 1$. Thus, the dominant contribution to the energy-emission rate at large ω comes from the temperature, which decreases as (see fig. 14)

$$T_H = T_H(0) \left(1 - \frac{(D-1)(D-4)\alpha}{2r_0^2}\right).$$

Therefore the energy-emission rate decreases exponentially with α

$$\frac{\partial^2 E}{\partial t \partial \omega} \approx \sum N_\ell \frac{\omega}{2\pi} e^{-\omega/T_H} \frac{\partial^2 E}{\partial t \partial \omega} \Big|_{\alpha=0} \times e^{-\omega(D-1)(D-4)\alpha/(2r_0^2 T_H)}.$$

Let us compare the Hawking radiation of Schwarzschild and GB black holes produced due to particle collisions of the same energy. The relation between the black hole mass M and its radius r_0 is given by

$$1 + \frac{(D-3)(D-4)\alpha}{2r_0^2} = \frac{8(M/M_*)\Gamma(\frac{D-1}{2})}{(r_0 M_*)^{D-3}(D-2)\pi^{(D-3)/2}}, \quad (25)$$

where M_* is the true fundamental scale of gravity. In units of the black hole horizon the energy-emission rate $\sim r_0^{-2}$. If we measure the black hole radius in units of TeV^{-1} , the energy-emission rate is measured in units of TeV^2 . In order to convert the energy-emission rate in the units of TeV/s , we divide it by the Plank constant $\hbar = 6.58 \cdot 10^{-28} TeV \cdot s$. For $\alpha = 0.1 M_*^{-2}$ and $D = 10$, the total energy-emission rate of GB black holes can be as much as 10^3 times smaller (see Fig. 11) than that of the Schwarzschild one. For other values of D the increase in the lifetime of black holes can be easily calculated in the same way.

Thus, we have shown that even small GB corrections to the D -dimensional Schwarzschild geometry lead to the great increasing of the lifetime of black holes, up to quite a few orders. This is certainly not enough for accreting of matter and thus is not dangerous for experiments in the LHC, yet, will produce a potentially observable effect.

Let us note that the suppression of the energy-emission rate at high ω due to the cooling of a black hole was observed in [11] for the Standard Model particles. Though the largest suppression of the graviton emission reported

in [11] is at $M \lesssim M_*$. In this regime however one cannot trust the solution (2), which is gravitationally unstable [20]. The other factor, the decreasing of the grey-body factors of the tensorial gravitons, strongly increased the suppression of the graviton emission at large D .

VI. CONCLUSIONS

We have shown that the widely accepted approximation of higher dimensional black holes by their classical Schwarzschild-Tangherlini model is not good, when one considers the Hawking radiation around a black hole. Intensive Hawking emission of gravitons, as well as of other particles, is suppressed by many orders, when one in-

cludes into consideration small quantum Gauss-Bonnet corrections. Consequently, lifetime of quantum corrected black holes is many orders larger than it is expected according to the current literature [25]. This makes further investigations of Hawking radiation of higher curvature corrected black holes appealing.

Acknowledgments

R. K. was supported by the *Alexander von Humboldt Foundation*, Germany. A. Z. was supported by *Fundação de Amparo à Pesquisa do Estado de São Paulo (FAPESP)*, Brazil.

-
- [1] P. Horava and E. Witten Nucl. Phys. B **460** 506 (1996).
 - [2] I. Antoniadis, Phys. Lett. B **246**, 377 (1990); N. Arkani-Hamed, D. Dimopoulos and G. Dvali G Phys. Lett. B **429** 263 (1998); Phys. Rev. D **59** 086004 (1999); I. Antoniadis, N. Arkani-Hamed, S. Dimopoulos and G. R. Dvali, Phys. Lett. B **436** (1998) 257 [arXiv:hep-ph/9804398]; L. Randall and R. Sundrum Phys. Rev. Lett. **83** 3370 (1999); Phys. Rev. Lett. **83** 4690 (1999).
 - [3] D. G. Boulware and S. Deser, Phys. Rev. Lett. **55**, 2656 (1985).
 - [4] R. Konoplya, Phys. Rev. D **71**, 024038 (2005) [arXiv:hep-th/0410057]; E. Abdalla, R. A. Konoplya and C. Molina, Phys. Rev. D **72**, 084006 (2005) [arXiv:hep-th/0507100]; A. Zhidenko, Phys. Rev. D **78**, 024007 (2008) [arXiv:0802.2262 [gr-qc]].
 - [5] S. W. Hawking, Commun. Math. Phys. **43**, 199 (1975).
 - [6] E. Jung and D. K. Park, Nucl. Phys. B **731**, 171 (2005). *Mod. Phys. Lett. A* **22**, 1635 (2007) [hep-th/0612043].
 - [7] S. Chen, B. Wang, R. K. Su and W. Y. Hwang, *JHEP* **0803**, 019 (2008) [arXiv:0711.3599 [hep-th]].
 - [8] J. A. Frost, J. R. Gaunt, M. O. P. Sampaio, M. Casals, S. R. Dolan, M. A. Parker and B. R. Webber, arXiv:0904.0979 [hep-ph].
 - [9] D. Ida, K. y. Oda and S. C. Park, *Phys. Rev. D* **71**, 124039 (2005); *Phys. Rev. D* **73**, 124022 (2006).
 - [10] H. Nomura, S. Yoshida, M. Tanabe and K. i. Maeda, *Prog. Theor. Phys.* **114**, 707 (2005).
 - [11] T. G. Rizzo, *Class. Quant. Grav.* **23**, 4263 (2006) [arXiv:hep-ph/0601029].
 - [12] J. Grain, A. Barrau and P. Kanti, *Phys. Rev. D* **72**, 104016 (2005) [arXiv:hep-th/0509128];
 - [13] V. Cardoso, M. Cavaglia and L. Gualtieri, *Phys. Rev. Lett.* **96**, 071301 (2006) [Erratum-ibid. **96**, 219902 (2006)] [arXiv:hep-th/0512002].
 - [14] P. Kanti, *Lect. Notes Phys.* **769**, 387 (2009) [arXiv:0802.2218 [hep-th]].
 - [15] P. Kanti, H. Kodama, R. A. Konoplya, N. Pappas and A. Zhidenko, *Phys. Rev. D* **80**, 084016 (2009) [arXiv:0906.3845 [hep-th]].
 - [16] B. F. Schutz and C. M. Will *Astrophys. J. Lett* **291** L33 (1985); S. Iyer and C. M. Will *Phys. Rev. D* **35** 3621 (1987); R. A. Konoplya, *Phys. Rev. D* **68**, 024018 (2003) [arXiv:gr-qc/0303052]; *J. Phys. Stud.* **8**, 93 (2004).
 - [17] R. A. Konoplya and A. Zhidenko, *Phys. Rev. D* **81**, 124036 (2010) [arXiv:1004.1284 [hep-th]]; *Phys. Lett. B* **686**, 199 (2010) [arXiv:0909.2138 [hep-th]].
 - [18] O. P. F. Piedra and J. de Oliveira, arXiv:1006.3802 [gr-qc]; R. A. Konoplya, *Phys. Lett. B* **679**, 499 (2009) [arXiv:0905.1523 [hep-th]]; M. l. Liu, H. y. Liu and Y. x. Gui, *Class. Quant. Grav.* **25**, 105001 (2008) [arXiv:0806.2716 [gr-qc]]; J. F. Chang, J. Huang and Y. G. Shen, *Int. J. Theor. Phys.* **46**, 2617 (2007); Y. Zhang and Y. X. Gui, *Class. Quant. Grav.* **23**, 6141 (2006) [arXiv:gr-qc/0612009]; H. T. Cho, A. S. Cornell, J. Doukas and W. Naylor, arXiv:0912.2740 [gr-qc]; R. A. Konoplya, K. Murata, J. Soda and A. Zhidenko, *Phys. Rev. D* **78**, 084012 (2008) [arXiv:0807.1897 [hep-th]].
 - [19] A. Ishibashi and H. Kodama, *Prog. Theor. Phys.* **110**, 901 (2003) [arXiv:hep-th/0305185]; H. Kodama and A. Ishibashi, *Prog. Theor. Phys.* **111**, 29 (2004) [arXiv:hep-th/0308128]; [arXiv:gr-qc/0312012]; R. A. Konoplya and A. Zhidenko, *Phys. Rev. D* **78**, 104017 (2008) [arXiv:0809.2048 [hep-th]]; *Phys. Rev. Lett.* **103**, 161101 (2009) [arXiv:0809.2822 [hep-th]]; *Nucl. Phys. B* **777**, 182 (2007) [arXiv:hep-th/0703231].
 - [20] G. Dotti and R. J. Gleiser, *Phys. Rev. D* **72**, 044018 (2005) [arXiv:gr-qc/0503117]; *Phys. Rev. D* **72**, 124002 (2005) [arXiv:gr-qc/0510069];
 - [21] T. Takahashi and J. Soda, [arXiv:1008.1618 [gr-qc]]; *Phys. Rev. D* **80**, 104021 (2009) [arXiv:0907.0556 [gr-qc]].
 - [22] R. A. Konoplya and A. Zhidenko, *Phys. Rev. D* **77**, 104004 (2008) [arXiv:0802.0267 [hep-th]].
 - [23] P. Kanti and J. March-Russell, *Phys. Rev. D* **66**, 024023 (2002) [arXiv:hep-ph/0203223]; *Phys. Rev. D* **67**, 104019 (2003) [arXiv:hep-ph/0212199]; P. Kanti, *Int. J. Mod. Phys. A* **19**, 4899 (2004) [arXiv:hep-ph/0402168].
 - [24] M. Casals, S. R. Dolan, P. Kanti and E. Winstanley, *JHEP* **0703**, 019 (2007) [arXiv:hep-th/0608193].
 - [25] F. Moura and R. Schiappa, *Class. Quant. Grav.* **24**, 361 (2007) [arXiv:hep-th/0605001]; S. Creek, O. Eftimiou, P. Kanti and K. Tamvakis, *Phys. Rev. D* **76**, 104013 (2007) [arXiv:0707.1768 [hep-th]]; *Phys. Lett. B* **635**, 39 (2006) [arXiv:hep-th/0601126]; V. Cardoso, M. Cavaglia and L. Gualtieri, *JHEP* **0602**, 021 (2006); [arXiv:hep-

th/0512116]; T. G. Rizzo, JHEP **0506**, 079 (2005) [arXiv:hep-ph/0503163]; J. L. Hewett, B. Lillie and T. G. Rizzo, Phys. Rev. Lett. **95**, 261603 (2005) [arXiv:hep-ph/0503178]; A. Barrau, J. Grain and

S. O. Alexeyev, Phys. Lett. B **584**, 114 (2004) [arXiv:hep-ph/0311238].